Spectroscopy and Redox Behaviour of Dicopper(II) and Dinickel(II) Complexes of Bis(cyclen) and Bis(cyclam) Ligands

Sanae El Ghachtouli,[a] Cyril Cadiou,[a] Isabelle Déchamps-Olivier,[a] Françoise Chuburu,*[a] Michel Aplincourt,[a] Véronique Turcry,[b] Michel Le Baccon,[b] and Henri Handel[b]

Keywords: Copper / Nickel / Bis(cyclen) ligands / Bis(cyclam) ligands / Electrochemistry / EPR spectroscopy

The dinuclear Cu^{II} and Ni^{II} complexes of *meta*-xylyl and pyridyl biscyclen and biscyclam have been prepared and characterised in solution by means of UV/Visible spectra, electrochemical and EPR studies. X-ray structures of copper biscyclen complexes have been obtained. The comparison of all the data shows that the potentially coordinating N(*py*) pyridyl atom promotes the interaction between the two metal centers, whether it is spontaneously coordinated (biscyclen complexes) or not (biscyclam ones).

Introduction

Tetraazamacrocyclic ligands like cyclen and cyclam are well known for their remarkable capacity to coordinate metallic ions. Their preorganisation, the flexibility of the macrocyclic framework and the soft character of the nitrogen donor atoms make the cyclic tetramines well suited for the complexation of d-block metals.[1] Thus, two of the properties of macrocyclic complexes that set them apart from the acyclic ones are selectivity in binding and kinetic stability with respect to dissociation. These features have been harnessed to develop macrocycles able to transport radioisotopic agents to a tumour site (^{64}Cu and ^{67}Cu for example).[2] Moreover, changes in the nitrogen (or carbon) substitution can determine their potential applications. In particular, functionalisation of cyclen by substituents such as acetate binding arms has led to a new class of ligands which are able to coordinate lanthanide cations especially Gd^{III}.[3] The corresponding complexes are developed and used as MRI contrast agents. Besides these medical applications, transition-metal complexes of tetraazamacrocycles in many respects, can be seen as metalloenzyme models, particularly when the ligand framework exhibits two or even three cavities. The corresponding bis- or tris-macrocycles may then be able to hold two or more metal centres in proximity, mimicking the multinuclear metal arrays at the active sites of the concerned metalloenzymes.[4] Since the length of the bridging groups controls the inter-metal ion distances, these ligands have been studied to examine the strength, more or less pronounced of the interaction between the metal centres. Kaden, Fabbrizzi and co-workers have shown through electrochemical and EPR studies of metallic bistetraazamacrocyclic complexes, that below an intermetallic distance of about 8 Å, metal–metal interactions can be detected.[5] In fact, in these studies the only parameter considered to tune the inter-metal distance is the spacer geometry. However, the flexibility of the macrocycle can induce favoured configurations of the cavity and then modifications of the metal coordination polyhedron. This factor may affect the intermetallic distance as well as topological modification of the ligand occurring during the redox process. Effectively, as recently shown for cyclam complexes the change in the metal redox state can be associated with their geometrical reorganisation.[6] Finally, the introduction of additional donor atoms on the intercycle spacer may interfere in the metal–metal distance due to selective coordination of one of the two metals to the linker.

In order to test the influence of these latter parameters, the preparation of dinuclear copper(II) and nickel(II) complexes based upon cyclen and cyclam cavities (Scheme 1) was improved and their electronic properties studied by means of electrochemical and EPR measurements.

Results and Discussion

Syntheses of Ligands and Complexes

The ligands $\mathbf{L^1}$ to $\mathbf{L^4}$ were synthesised according the bisaminal methodology[7] and the corresponding dinuclear complexes were obtained by addition of equimolar amounts of metallic salts (ClO_4 or BF_4 salts – see experimental section). Monocrystals suitable for an X-ray analysis were obtained for the copper complexes of cyclen ligands $\mathbf{L^1}$ and $\mathbf{L^2}$.

[a] GRECI, Université de Reims Champagne–Ardenne, B. P. 1039, 51687 Reims Cedex 2, France
[b] UMR CNRS 6521, Université de Bretagne Occidentale, B. P. 809, 29285 Brest Cedex, France
E-mail: francoise.chuburu@univ-reims.fr
Supporting information for this article is available on the WWW under http://www.eurjic.org or from the author.

  DOI: 10.1002/ejic.200500120

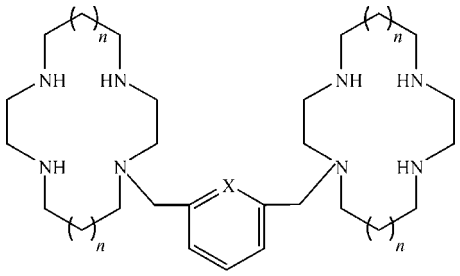

X = **C**, *n* = **0** biscyclen-meta: **L**[1]

X = **N**, *n* = **0** biscyclen-pyridine: **L**[2]

X = **C**, *n* = **1** biscyclam-meta: **L**[3]

X = **N**, *n* = **1** biscyclam-pyridine: **L**[4]

Scheme 1.

Structural Characterisation in the Solid State of Complexes $[Cu_2L^{1,2}]$

POV-ray depiction of $[Cu_2L^1]^{4+}$ complex is provided in Figure 1. The monocrystals were isolated by slow diffusion of a saturated sodium perchlorate solution into an aqueous solution of the complex. They show that two copper ions are coordinated by the four macrocyclic nitrogen atoms of each cyclen cavity and by a water molecule, leading to two pentacoordinate subunits linked together by a metaxylyl bridge. Selected bond lengths and angles are shown in Table 1. The Cu–NH bond lengths [2.016(5)–2.031(5) Å] are close to the ones in bis-*para*xylyl cyclen copper complex[8] while the bonds to the tertiary macrocyclic nitrogens are slightly longer [2.035(5)/2.046(5)] Å. This is certainly the consequence of the *N*-alkylation on these atoms as it is known that the M–N bond lengths are increased by *N*-alkyl substitution.[8–10] The copper coordination spheres are completed by oxygen donors from water molecules (one per copper ion) with Cu–O bond lengths of [2.142(4)/2.160(5)] Å. For each copper ion, the resulting geometry is based on a square planar pyramid, the metal ion being approximately at a distance of 0.50 Å from the base of the pyramid. At last for this complex, the intramolecular Cu–Cu distance is measured at 9.713 Å, while shorter intermolecular Cu–Cu distances are observed (7.333, 8.274, 9.582 Å).

The X-ray structure of the copper(II) complex of **L**[2] is provided in Figure 2 and relevant geometry details in Table 2. Monocrystals were grown by slow diffusion of diethylether in an acetonitrile solution of the tetrafluoroborate copper complex. Crystallographic analysis of $[Cu_2L^2(BF_4)](BF_4)_3$ shows the two copper ions to be pentacoordinate as expected for copper held in a cyclen cavity. The crystal structure underlines that the pyridyl nitrogen atom [N(*py*)] allows the discrimination of the two cavities since this atom is coordinated to only one of the two copper ions. Thus, the Cu(1) atom is bonded to the four nitrogen atoms of the first macrocyclic cavity [Cu–NH: from 2.019(7) to 2.033(7) Å; Cu–NR: 2.041(6) Å] and at a greater distance by the nitrogen atom of the pyridine ring [Cu–N(*py*): 2.266(6) Å]. The coordination of the N(*py*) atom certainly allows the formation of an efficient five-membered chelate ring which geometrically leads to a smaller N(*py*)-Cu–N angle, of 80.4(1)° for the N_1 nitrogen carrying the pyridine linker, compared to values of 95.4(3) to 129.6(3)° for the other three N(*py*)-Cu–N angles. In parallel, the Cu(2) atom is coordinated to the four nitrogen atoms of the second macrocyclic cavity [Cu–NH: from 2.021(7) to 2.038(7) Å; Cu–NR: 2.064(6) Å] and to a tetrafluoroborate anion [Cu–F: 2.135(6) Å]. The distances of the copper ions with regard to their corresponding macrocyclic cavities are about 0.54 Å (CuN_5 chromophore) or 0.51 Å (CuN_4 chromophore). The main consequence of the N(*py*) atom coordination to one of the two copper ions is the significant shortening of the intramolecular Cu–Cu distance since it is

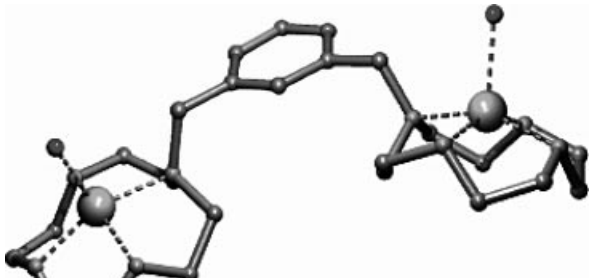

Figure 1. POV-ray diagram of $[Cu_2L^1(H_2O)_2]^{4+}$.

Table 1. Bond lengths [Å] and angles [°] in $[Cu_2L^1]^{4+}$.

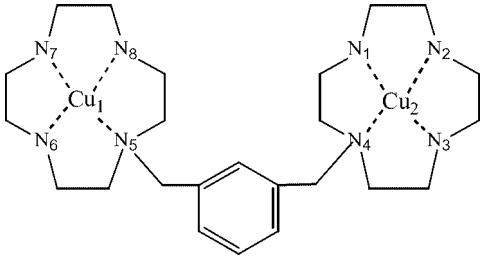

Cu1–O1	2.142(4)	O1–Cu1–N1	104.6(2)
Cu1–N1	2.019(5)	O1–Cu1–N2	104.4(2)
Cu1–N2	2.016(5)	O1–Cu1–N3	105.6(2)
Cu1–N3	2.029(5)	O1–Cu1–N4	103.0(2)
Cu1–N4	2.046(5)	N1–Cu1–N2	86.4(2)
Cu2–O2	2.160(5)	N1–Cu1–N3	149.9(2)
Cu2–N5	2.035(5)	N1–Cu1–N4	87.0(2)
Cu2–N6	2.031(5)	N2–Cu1–N3	86.2(2)
Cu2–N7	2.026(5)	N2–Cu1–N4	152.6(2)
Cu2–N8	2.022(5)	N3–Cu1–N4	86.3(2)
		O2–Cu2–N5	108.6(2)
		O2–Cu2–N6	106.9(2)
		O2–Cu2–N7	98.1(2)
		O2–Cu2–N8	102.3(2)
		N5–Cu2–N6	86.5(2)
		N5–Cu2–N7	153.3(2)
		N5–Cu2–N8	86.0(2)
		N6–Cu2–N7	86.6(2)
		N6–Cu2–N8	150.8(2)
		N7–Cu2–N8	87.6(2)

decreased to 5.779 Å. This distance is the shortest intermetallic one in the crystal. Compared to the $[Cu_2\mathbf{L^1}]^{4+}$ complex, $[Cu_2\mathbf{L^2}(BF_4)](BF_4)_3$ could be better for the observation of metal–metal interactions.

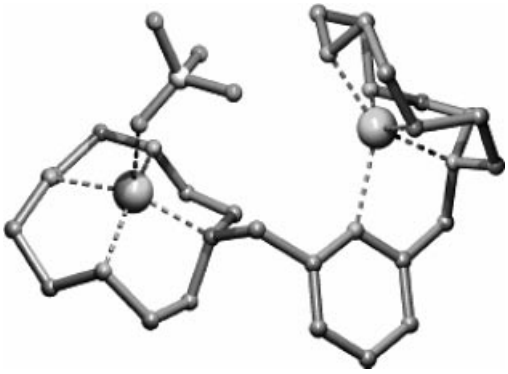

Figure 2. POV-ray diagram of $[Cu_2\mathbf{L^2}(BF_4)]^{3+}$.

Table 2. Bond lengths [Å] and angles [°] in $[Cu_2\mathbf{L^2}]^{4+}$.

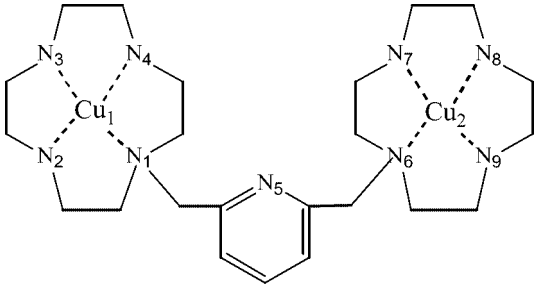

Cu1–N1	2.041(6)	N1–Cu1–N2	86.8(3)
Cu1–N2	2.030(7)	N1–Cu1–N3	149.4(3)
Cu1–N3	2.033(7)	N1–Cu1–N4	85.5(3)
Cu1–N4	2.019(7)	N1–Cu1–N5	80.4(2)
Cu1–N5	2.266(6)	N2–Cu1–N3	85.5(3)
Cu2–N6	2.064(6)	N2–Cu1–N4	148.5(3)
Cu2–N7	2.029(7)	N2–Cu1–N5	113.3(3)
Cu2–N8	2.038(7)	N3–Cu1–N4	85.9(3)
Cu2–N9	2.021(7)	N3–Cu1–N5	129.6(3)
Cu2–F	2.135(6)	N4–Cu1–N5	95.4(3)
		N6–Cu2–N7	86.9(3)
		N6–Cu2–N8	151.7(3)
		N6–Cu2–N9	86.2(3)
		N6–Cu2–F	109.1(3)
		N7–Cu2–N8	86.2(3)
		N7–Cu2–N9	149.4(3)
		N7–Cu2–F	102.7(3)
		N8–Cu2–N9	85.8(3)
		N8–Cu2–F	99.2(3)
		N9–Cu2–F	107.7(3)

Solution Properties

Electronic Absorption Spectroscopy

The UV/Visible absorption maxima of the complexes $[Cu_2\mathbf{L}]^{4+}$ and $[Ni_2\mathbf{L}]^{4+}$ ($\mathbf{L} = \mathbf{L^{1-4}}$) in water and acetonitrile are given as supporting information.

Copper Complexes: As commonly observed for these compounds, the featureless nature of the spectra makes difficult a detailed description of coordination geometries. Nevertheless, the main information resulting from the visible spectra of the copper biscyclen complexes ($[Cu_2\mathbf{L^{1,2}}]^{4+}$) are the following: for $[Cu_2\mathbf{L^1}]^{4+}$ whatever the solvent, the spectrum exhibits a broad band at 594 nm typical of a square based pyramidal copper complex (CuN_4S chromophore, S = solvent).[8] For $[Cu_2\mathbf{L^2}]^{4+}$, the spectrum is dissymmetrical and its deconvolution analysis shows that it is the superimposing of two spectra, the first one characteristic of a CuN_4S chromophore (with a band at 584–594 nm), the second one attributed to a CuN_5 chromophore[11] (shoulder between 684 and 735 nm, according to the solvent). Moreover, the presence of this shoulder indicates that the coordination of the pyridyl nitrogen N(*py*) to the copper ion is maintained in solution, whatever the pH conditions.

For the cyclam copper complexes $[Cu_2\mathbf{L^{3,4}}]^{4+}$, the absorption maxima at about 520 nm are typical of square planar copper complexes.[12] The lack of absorption at about 650 nm[13] is indicative of an absence of interaction between the pyridyl nitrogen atom N(*py*) and a copper ion for the $[Cu_2\mathbf{L^4}]^{4+}$ complex.

Nickel Complexes: For the nickel biscyclen complexes ($[Ni_2\mathbf{L^{1,2}}]^{4+}$) the UV/Visible spectra are indicative of octahedral coordination for the nickel in solution, solvent molecules occupying the free positions of the octahedron (chromophore NiN_4S_2).[14] Two bands are observed for both complexes in water and in acetonitrile corresponding to the predicted $^3A_{2g} \rightarrow {}^3T_{2g}$ (950–800 nm) and $^3A_{2g} \rightarrow {}^3T_{1g}$ (F) (560–500 nm) transitions for a d^8 metal ion under octahedral symmetry, the third transition $^3A_{2g} \rightarrow {}^3T_{1g}$ (P) (300–400 nm) being hidden by the stronger absorbance of the ligand ($\lambda < 300$ nm).

For the nickel cyclam complexes ($[Ni_2\mathbf{L^{3,4}}]^{4+}$), the solution visible spectra show a single band with the maximum in the range 450–470 nm, depending on both the complexes and the solvent. This signal is in accordance with the $[Ni(cyclam)]^{2+}$ spectrum ($\lambda = 459$ nm) and is consistent with the adoption by the metal of a square-planar geometry, the metal being perfectly fitted inside the macrocyclic cavity. In solution, the coexistence for $[Ni(cyclam)]^{2+}$complexes of square planar (low spin) and octahedral (high spin) geometries is well documented leading to a "yellow to blue" equilibrium between these species.[15] For the $[Ni_2\mathbf{L^{3,4}}]^{4+}$ complexes, we were not able to detect any additional peaks corresponding to octahedral nickel(II) ions. Two reasons may be responsible for that: either no octahedral complexes are present in solution or, because of low molar extinction coefficients, the octahedral complexes are difficult to detect. Finally, for $[Ni_2\mathbf{L^4}]^{4+}$, whatever the solvent and the pH conditions, the spectrum is identical and in addition similar to the one of $[Ni_2\mathbf{L^3}]^{4+}$. As for its copper homologue, this is indicative of an absence of interaction between the pyridyl nitrogen atom N(*py*) and the nickel.

Electrochemical Properties of the Bismacrocyclic Complexes

The binuclear $[Cu_2\mathbf{L}]$ and $[Ni_2\mathbf{L}]$ complexes ($\mathbf{L} = \mathbf{L^{1-4}}$) were all investigated by cyclic voltammetry in CH_3CN, the

working electrode being a glassy carbon disk and the Fc^+/Fc couple being used as a reference in acetonitrile.

Biscyclen Complexes: The cyclen cavity is not well adapted to stabilize +I and +III oxidation states for copper and nickel.[16] Therefore, it was not possible to obtain reproducible voltammograms, mainly because of the degradation of oxidised and reduced forms during the experiment.

Biscyclam Complexes: The copper complexes $[Cu_2\mathbf{L^3}]^{4+}$ and $[Cu_2\mathbf{L^4}]^{4+}$ show two irreversible bielectronic exchanges (one electron per metallic centre) separated by $\approx$ 2.40 V (Table 3). The anodic peaks happen respectively for $[Cu_2\mathbf{L^3}]^{4+}$ and $[Cu_2\mathbf{L^4}]^{4+}$at 1.25 V and 1.15 V while the cathodic ones happen at –1.21 V and –1.22 V. These values are in accordance with the ones measured for the monomeric [Cu(cyclam)]$^{2+}$ (1.02 V and –1.28 V), taking into account the incidence of the *N*-alkylation of the macrocyclic cavity on the redox potentials.[5d,17] In reduction, the two copper complexes exhibit a similar behaviour i.e. the $Cu^{II/I}$ process is irreversible and the reverse process is accompanied by a partial release of the metal, reported by an anodic peak at –0.60 V (Cu^0). In oxidation, the forward and reverse peak heights are inequivalent ($i_a >> i_c$), indicating that the electronic exchange $Cu^{II/III}$ is irreversible too. Moreover, the high anodic current wave detected for the first cycle, the decrease of its intensity when the number of cycles increased, and the apparition of a deposit at the electrode during the experiment show that the oxidated species $[Cu_2\mathbf{L^{3,4}}]^{6+}$ are highly unstable and react rapidly in the medium. This is consistent with observations generally done with copper tetraazamacrocyclic complexes.[18] We have checked that, as demonstrated by Fabbrizzi et al.,[5d] in concentrated perchloric acid solution (70%) at a Pt electrode, the Cu^{III} bistetraazamacrocyclic complexes become stable, at least at the time scale of the voltammetry experiment. In this special medium, the oxidation process is effectively quasi reversible ($i_a = i_c$). In order to have a greatest resolution of the signals associated with the consecutive redox events ($Cu^{II}\ Cu^{II} \rightarrow Cu^{II}\ Cu^{III} \rightarrow Cu^{III}\ Cu^{III}$) whose potentials are not very distant,[5d] differential pulse voltammetry (DPV) was used. The DPV profiles obtained for the two complexes in the oxidation scan are similar and exhibit a single wave peak. The measurements reproduce well the one already done by Fabbrizzi et al.[5d] for the $[Cu_2\mathbf{L^3}]^{4+}$ complex and indicate that for these two complexes the ring-to-ring distance is certainly too long to induce a two consecutive one-electron steps process.

Table 3. Electrochemical parameters for the $Cu_2\mathbf{L^3}$ and $Cu_2\mathbf{L^4}$ complexes.

	Oxidation potential	Reduction potential
$Cu_2\mathbf{L^3}$ (CH_3CN)[a]	E_p = 1.25 V	E_p = –1.21 V
$Cu_2\mathbf{L^4}$ (CH_3CN)[a]	E_p = 1.15 V	E_p = –1.22 V
$Cu_2\mathbf{L^3}$ ($HClO_4$, 70%)[b]	$E_{1/2}$ = 0.98 V (0.10 V)	–
$Cu_2\mathbf{L^4}$ ($HClO_4$, 70%)[b]	$E_{1/2}$ = 1.02 V (0.10 V)	–

[a] Potential values are given vs. Fc^+/Fc. [b] Potential values are expressed vs. SCE.

Cyclic voltammograms recorded for the nickel complexes $[Ni_2\mathbf{L^3}]^{4+}$ and $[Ni_2\mathbf{L^4}]^{4+}$ are reported in Figure 3. In reduction, the behaviour of the two complexes is quasi reversible and the $Ni^{II/I}$ system is electrochemically slow. The oxidation of the two complexes is more complicated since more than one CV wave is observed. Thus, for the complex $[Ni_2\mathbf{L^3}]^{4+}$ two oxidation potentials at 0.80 and 1.12 V are detected while the complex $[Ni_2\mathbf{L^4}]^{4+}$ shows two oxidation processes, the first one at 0.84 V and the second one split into two peaks at 1.03 and 1.18 V. For $[Ni_2\mathbf{L^3}]^{4+}$ the two CV waves are quasi reversible while for $[Ni_2\mathbf{L^4}]^{4+}$, the reversibility of the first system is very poor. It is noticeable that previous voltammetry experiments carried out for $[Ni_2\mathbf{L^3}]^{4+}$ [5d] have shown a simple oxidative behaviour since only the first system (0.80 V) was detected. As the purity of our complexes is satisfactory, one can think that in CH_3CN, two bismacrocyclic Ni^{II} species are successively oxidised. In $[Ni_2\mathbf{L^3}]^{4+}$ complex, the proportion of these two species is largely in favour of the first one while in $[Ni_2\mathbf{L^4}]^{4+}$ the proportion is similar. In CH_3CN, an increase of the temperature (298 K up to 313 K) results in growth of the second system at the expense of the first one (Figure 4a). When the CV waves are recorded at temperatures of 298 K down to 233 K (Figure 4b, Figure 5b), for both complexes the second system tends to disappear. It is also noticeable that for $[Ni_2\mathbf{L^4}]^{4+}$ the first system becomes more reversible. From these observations, it can be assumed that the oxidation of the first species is followed by a rearrangement. A temperature decrease can prevent this isomerisation and the vanishing at lower temperatures of the second oxidative system, would tend to show that the two oxidative processes are dependent on each other. As far as nickel(II) cyclam complexes are concerned, several stereoisomers have to be considered, according to the configuration of the macrocyclic cavity (Figure 6). There are five possible configurational isomers of planar complexes of the macrocyclic ligand cyclam:[19] RSRS (++++) i.e. type I, RSRR (+-++) i.e. type II, RRSS (+--+) i.e. type III, RSSR (++--) i.e. type IV, RRRR (+-+-) i.e. type V, where + indicates that the hydrogen of the NH is above the plane of the macrocycle and - indicates that it is below the plane.

A cluster analysis of Ni-14 membered tetraazamacrocycles found in the Cambridge Structural database[20] shows that the most frequent configurations encountered for these complexes are the type I and type III ones; the amount of these two forms can moreover vary according to the coordination shell geometry of the nickel and the macrocycle substitution. On certain conditions, isomerisation between type I and type III structures have been evidenced: for instance, the oxidatively induced isomerisation of type I [Ni(cyclam)]$^{2+}$ into type III has been reported,[6a] while in bistetraazamacrocyclic series, the isomerisation of the type III [Zn_2 (bis *para*-cyclam)] complex into the type I[21] has been described. Such an isomerisation can be proposed for the $[Ni_2\mathbf{L^3}]^{4+}$ and $[Ni_2\mathbf{L^4}]^{4+}$complexes. Unfortunately, the impossibility to isolate and characterise independently the supposed type III and type I isomers prevents any kinetic quantitative study of the equilibrium between these two

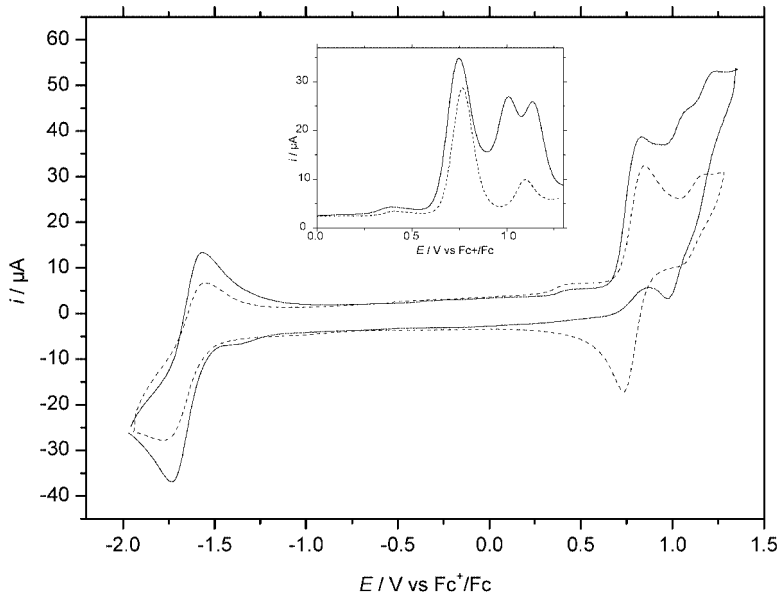

	$E_{½}$ox (ΔE_p)	$E_{½}$red (ΔE_p)
$[Ni_2\mathbf{L^3}]^{4+}$ (CH_3CN)[a]	0.80 V (0.10 V)	-1.66 V (0.19V)
	1.12 V (0.11 V)	
$[Ni_2\mathbf{L^4}]^{4+}$ (CH_3CN)[a]	0.84 V (irrev)	-1.65 V (0.17 V)
	1.03 V (0.11 V)	
	1.18 V (0.10 V)	

Figure 3. Cyclic voltammetry at a glassy carbon disk (CH_3CN/Bu_4NPF_6, c = 0.1 mol L^{-1}; v = 100 mV s^{-1}) of millimolar solutions of $[Ni_2\mathbf{L^3}]^{4+}$ (dashed lines) and $[Ni_2\mathbf{L^4}]^{4+}$ (straight lines) and Differential Pulse Voltammetry of their oxidation system (10 mV step potential).

configurations. However, the variation of the CV traces with the scan sweep rate can be indicative (Figures 4c and 5a). Comparison of the CV traces shows that for $[Ni_2\mathbf{L^4}]^{4+}$ the increase of the sweep rate improves the reversibility of the first system. Moreover, during the same experiments, the second system is affected since it tends to disappear for both complexes. It is interesting to notice that changes observed by increasing the CV sweep rate are similar to the changes previously noted by lowering the temperature (Figure 4b and Figure 5b). It led us to propose a configurational equilibrium in solution, slightly shifted upon electrochemical oxidation between the type III and the type I isomers of $[Ni_2\mathbf{L^3}]^{4+}$ and $[Ni_2\mathbf{L^4}]^{4+}$ biscyclams. Voltammetric data alone cannot bring any geometrical information about the coordination shell and it is difficult to identify the structures formed upon the oxidation. However, by comparison of the gap between redox potentials determined for type III and type I isomers of [Ni(cyclam)]$^{2+}$[6a] one can propose for $[Ni_2\mathbf{L^3}]$ that the first system ($E_{½ox}$ = 0.80 V) corresponds to the oxidation of the two Ni ions held in a type III cavity while the second system ($E_{½ox}$ = 1.12 V) corresponds to the oxidation of the two Ni ions held in a type I cyclam cavity. The oxidative process can then be modelled as a classical square scheme, involving the electron-transfer reactions and the isomerisation processes (Scheme 2): the first oxidation peak corresponds to the electrogeneration of the type III $[Ni_2\mathbf{L^3}]^{6+}$ complex that undergoes a partial rearrangement to form the type I $[Ni_2\mathbf{L^3}]^{6+}$. Since the potential corresponding to the generation of the type I $[Ni_2\mathbf{L^3}]^{6+}$ is more positive than the redox potential of the $Ni^{II/III}$ in the type III complex, type I $[Ni_2\mathbf{L^3}]^{6+}$ species is immediately reduced into type I $[Ni_2\mathbf{L^3}]^{4+}$ species; this species is further oxidised at a more positive potential. This implies that the isomerisation process requires an elongation of the metal–nitrogen bonds of the tetraazamacrocycle, which readily takes place

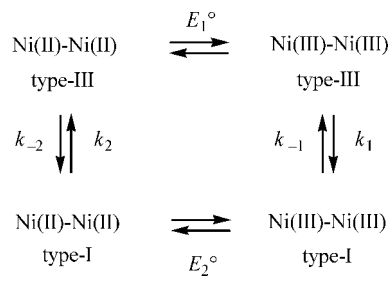

Scheme 2.

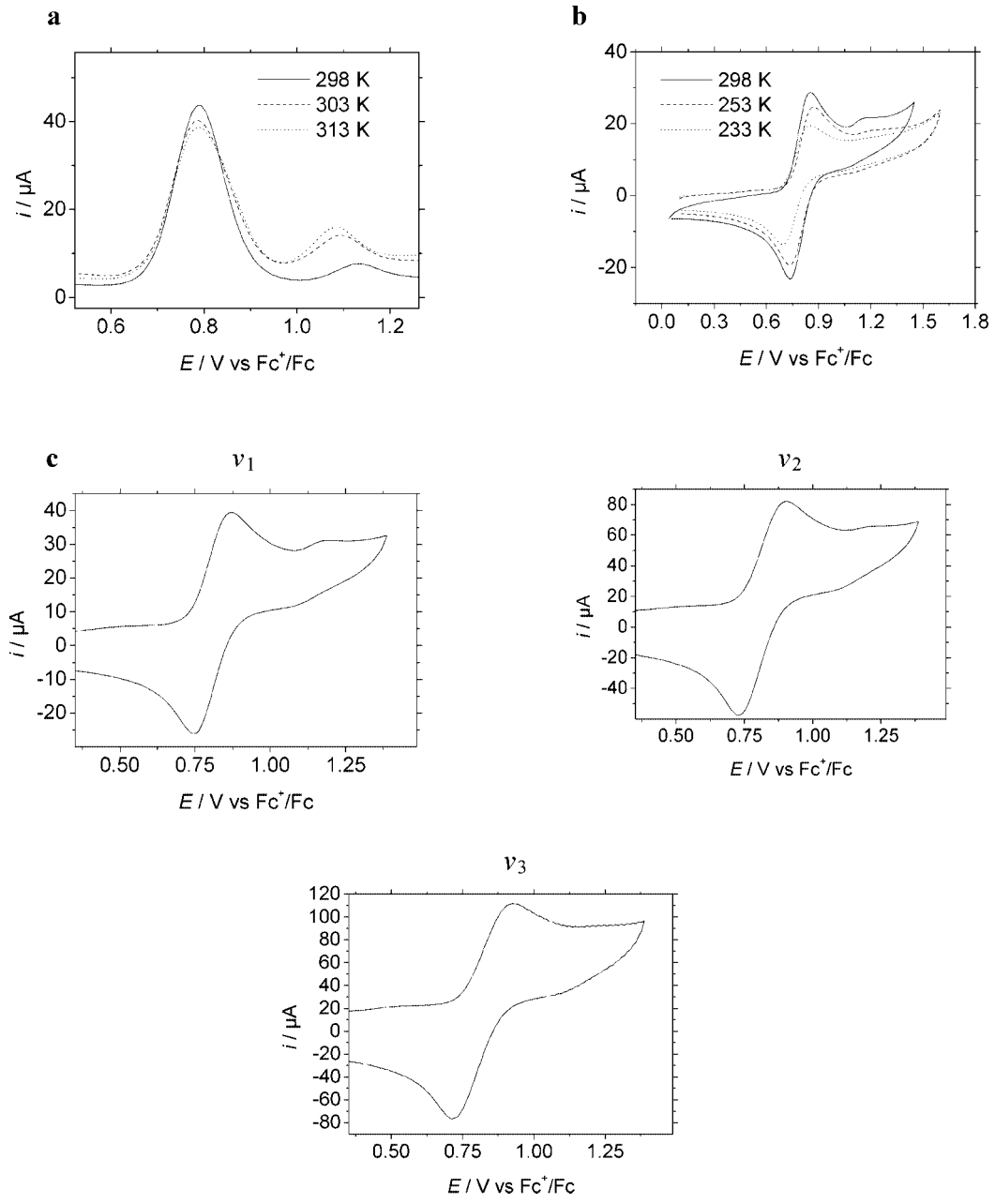

Figure 4. a: DPV profiles. b: CV curves of $[Ni_2\mathbf{L^3}]^{4+}$ at different temperatures. c: CV curves at v_1 = 100 mV s^{-1}, v_2 = 500 mV s^{-1}, v_3 = 1000 mV s^{-1}.

on cyclam derivatives by modification of the electron density on the metal, induced by the electrochemical oxidation $Ni^{II/III}$. Consequently, such isomerisation is negligible in acetonitrile without an electrochemical oxidation-reduction cycle. For complex $[Ni_2\mathbf{L^4}]^{4+}$, the electronic process is certainly more complicated than suggested by the square scheme since the oxidation peak of the supposed type I isomer is split. At this stage, only hypothesis can be formulated to interpret this signal. On the course of the (type III → type I) isomerisation process, a modification of the metal coordination sphere takes place as previously said. At the next step, the coordination of the nitrogen atom of the pyridine linker can occur on one of the two nickel centres, to lead to the oxidable type I $[Ni_2\mathbf{L^4}]^{4+}$ entity. This assumption is supported by the fact that most of the type I Ni^{II} complexes based on cyclam cavities are known to exhibit whether in a square planar or a square pyramidal configuration.[13,20] To test this proposal, modelling of type I $[Ni_2\mathbf{L^4}]^{4+}$ was improved in order to check the preferential equilibrium geometry of the complex. Whatever the type I starting geometry [N(*py*) coordinated or not], the most stable configuration corresponds to a situation where the nitrogen pyridyl atom is coordinated to one of the two nickel metals (Figure 7). Moreover, insofar as we can trust these calculations (because of the system size, the calculation level is restricted) the pyridinic nitrogen atom brings

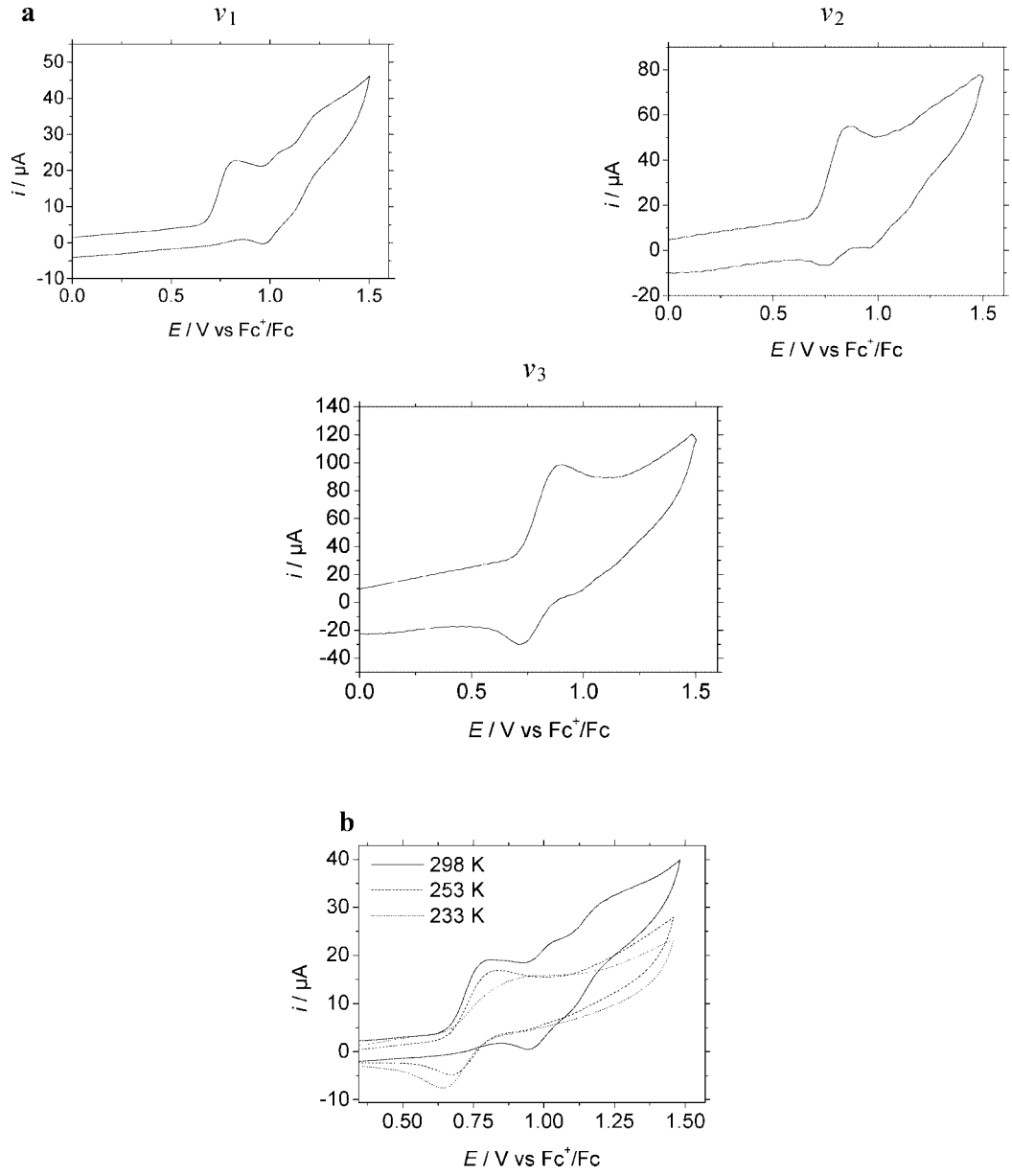

Figure 5. CV curves of $[Ni_2\mathbf{L^4}]^{4+}$. a: v_1 = 100 mV s^{-1}, v_2 = 600 mV s^{-1}, v_3 = 2000 mV s^{-1}. b: at different temperatures.

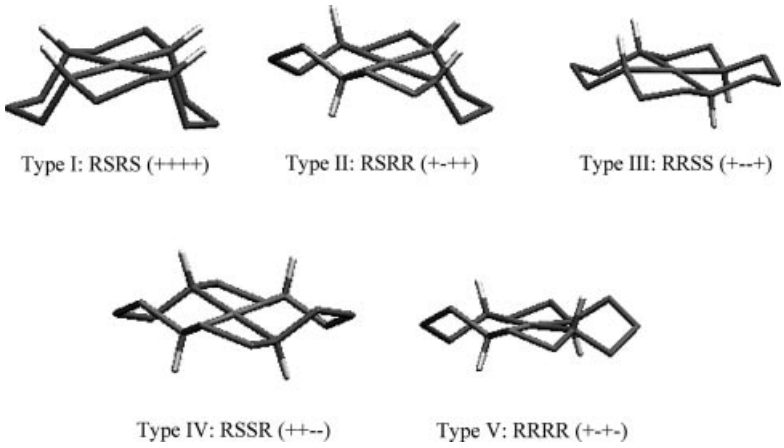

Figure 6. Five possible configurational isomers of planar complexes of the macrocyclic ligand cyclam.

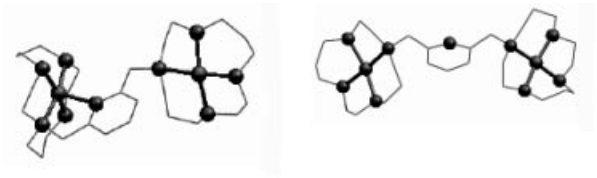

E_F(UHF/LANL2MB)	0	42.47 kcal mol^{-1}
E_F (UB3LYP/LANL2DZ)	0	38.42 kcal mol^{-1}
d (Ni ... N*py*)	2.271Å / 5.419 Å	5.351Å / 5.319 Å
d (Ni ... Ni)	6.865 Å	10.251 Å

Figure 7. Relative energies of formation (kcal mol^{-1}) and main geometrical parameters of type I isomers of $[Ni_2\mathbf{L^4}]^{4+}$ complexes (on the structures, hydrogen atoms are omitted for clarity).

the macrocycles and the metallic ions nearer (6.86 Å). Consequently, the two distinct peaks of the type I oxidation system can be assigned either to two different coordination modes of the two nickel ions (respectively NiN_5 and NiN_4) or to consecutive monoelectronic processes, the first one being assigned to the $Ni^{II/III}$ process at one of the metal centres, the second one to be ascribed to the one-electron oxidation at the other metal centre. Even if this last interpretation was previously proposed for a [Ni_2(biscyclam)] complex[5b] in which the metal centres are separated by 7.09 Å, none of these two propositions can be ruled out on the basis of electrochemical experiments.

EPR Spectroscopy of the Bismacrocyclic Complexes

The EPR spectra of the $[Cu_2\mathbf{L^{1-4}}]^{4+}$ complexes were recorded in DMF solution at 100 K in order to determine their *g* and *A* parameters (Figure 8). The simulated anisotropic EPR parameters are listed in Table 4. By way of comparison, the EPR parameters of the known acetate complexes $[Cu_2\mathbf{L^{1,3}}]^{4+}$[22] are also reported.

The X-band EPR spectra of frozen solutions exhibit a strong absorption at ≈ 3200 G, attributable to the allowed transitions $\Delta M_S = 1$. For the cyclam complexes $[Cu_2\mathbf{L^{3,4}}]^{4+}$ the EPR parameters are similar which means that the copper ions are held in an identical environment. The $g_{\|}$ values are found to be the same for both complexes, namely 2.182. These values are greater than the *g* ones, which is typical of axially symmetric d^9 copper complexes and a $d_{x^2-y^2}$ ground state.[23] The hyperfine coupling constants $A_{\|}$ (100 10^{-4} cm^{-1}) are as expected,[8,22] about half the value of the mononuclear complexes, in which the metal is held in a square planar environment. In the parallel region, the hyperfine system shows seven lines. This signal is typical of copper(II) dimers weakly coupled and can be interpreted as a triplet state spectrum originating from exchange-coupled pairs of copper(II) ions.[22] Thus, two series of seven lines are theoretically expected,[24] one for each allowed ΔM_S = 1 transition; they correspond to the hyperfine coupling between the two copper d^9 ions (I_{Cu} = 3/2). According to the zero-field splitting amplitude, the two septets can either overlap (weak D factor) or be shifted, even if in this case it is difficult to observe all the lines.[4c,5b] The simulation[25] of

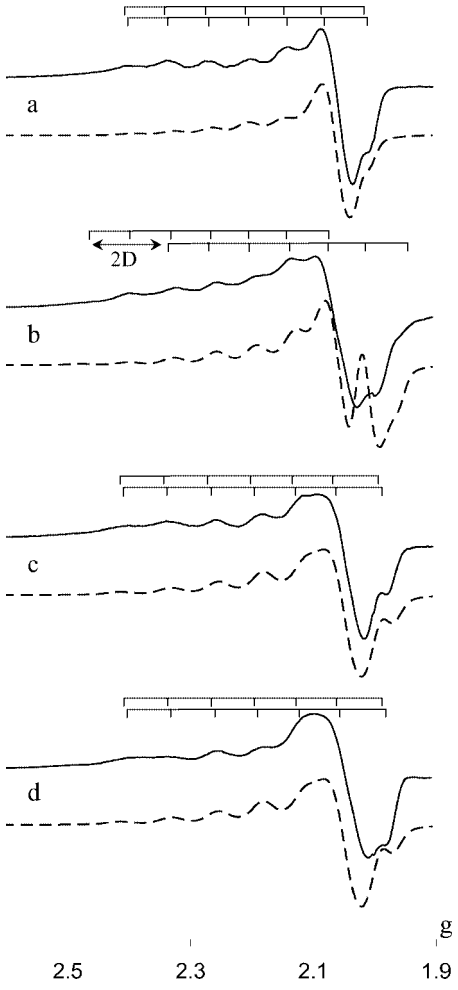

Figure 8. Experimental EPR spectra of biscyclen complexes. a: $[Cu_2\mathbf{L^1}](BF_4)_4$. b: $[Cu_2\mathbf{L^2}](BF_4)_4$ and of biscyclam complexes. c: $[Cu_2\mathbf{L^3}](BF_4)_4$. d: $[Cu_2\mathbf{L^4}](BF_4)$. Dotted spectra: simulated EPR spectra.

the spectrum can then help for the interpretation of the signals: for the complexes $[Cu_2\mathbf{L^{3,4}}]^{4+}$, the simulated spectra tend to demonstrate that the two septets overlap. This means that the exchange interaction between the two copper ions is weak. Nevertheless, the Cu^{II}–Cu^{II} interaction is present as shown by the existence of more than four hyperfine lines in the spectra of the $[Cu_2\mathbf{L^{3,4}}]^{4+}$ complexes and by

Table 4. EPR parameters of $[Cu_2\mathbf{L^{1-4}}]$ complexes in frozen solution (DMF) at 100 K.

	$g_{\parallel}$	$g_{\perp}$	$A_{\parallel}$ [10^{-4} cm^{-1}]	$D_{\parallel}$ [10^{-4} cm^{-1}][a]
$[Cu_2\mathbf{L^1}]^{4+}$[b]	2.207	2.065	81	8
$[Cu_2\mathbf{L^1}]^{4+}$[c]	2.20	2.07	102	
$[Cu_2\mathbf{L^2}]^{4+}$[b]	2.193	2.03	90	90
$[Cu(cyclen)]^{2+}$[d]	2.198	2.057	184	
$[Cu_2\mathbf{L^3}]^{4+}$[b]	2.182	2.05	100	8
$[Cu_2\mathbf{L^3}]^{4+}$[c]	2.19	2.06	107	
$[Cu_2\mathbf{L^4}]^{4+}$[b]	2.182	2.05	100	8
$[Cu(cyclam)]^{2+}$[d][24]	2.186	2.049	205	

$$r = \sqrt[3]{\frac{0.65\, g_{\parallel}^2}{D_{\parallel}}} \qquad (1)$$

[a] Parameter obtained by simulation (Simfonia).[25] [b] This work. [c] Ref.[22] [d] Ref.[12].

smaller values for $A_{\parallel}$.[4c,5,8,22,24] For an analogous series of xylyl-bismacrocyclic dicopper acetate complexes,[22] a second weak absorption at $\approx$ 1550 G was previously reported and assigned to the forbidden $\Delta M_S = 2$ transition. This transition was claimed as a further proof of intramolecular electron exchange between the two copper ions. Unfortunately, we were not able to highlight this signal for the two complexes $[Cu_2\mathbf{L^{3,4}}]^{4+}$ certainly because in these compounds the presence of a noncoordinating anion (BF_4^-) in solution prevents any strengthening of such interaction between the metal ions.

For the cyclen complexes $[Cu_2\mathbf{L^{1,2}}]^{4+}$, the comparison of the EPR parameters with the ones of the mononuclear $[Cu(cyclen)]^{2+}$ shows that $g_{\parallel}$ and $g_{\perp}$ are similar for all complexes. As already described for the cyclam complexes, the $A_{\parallel}$ values of $[Cu_2\mathbf{L^{1,2}}]^{4+}$ are half that determined for mononuclear $[Cu(cyclen)]^{2+}$. Moreover, the $g_{\parallel}$ parameters of $[Cu_2\mathbf{L^{1,2}}]^{4+}$ are higher than the ones of the cyclam analogues. This indicated that the coordination Scheme of copper ions in cyclen and cyclam is different. It is confirmed by the $A_{\parallel}$ values since, in cyclen complexes, the hyperfine coupling constants are smaller than the cyclam ones. It corresponds to a coordination of the copper ions outside the cyclen cavity, which is consistent with the crystal structure and the UV/Visible spectra of the complexes. Interestingly, the EPR spectrum of the pyridyl $[Cu_2\mathbf{L^2}]^{4+}$ complex exhibits more than seven lines in the parallel region. The simulated spectrum allows the proposal of an hyperfine system of nine lines. In this case, we assumed that the two septets are shifted by zero-field splitting 2D[24] and the simulation of the spectrum allowed the determination of a $D_{\parallel}$ parameter of 90 10^{-4} cm^{-1}. This value is tenfold increased compared to the ones simulated for the other complexes. This means that in the pyridyl $[Cu_2\mathbf{L^2}]^{4+}$ complex, the interaction between the metallic centres is stronger. From the D value, one can estimate the mean distance between the two paramagnetic cations, provided that the zero-field splitting is due to a pure dipole–dipole interaction:[24] from Equation (1) (Table 4), one obtains r_{Cu-Cu} = 7.03 Å for complex $[Cu_2\mathbf{L^2}]^{4+}$ in frozen DMF solution. This would indicate that in solution, the probable coordination of the pyridyl nitrogen shown by UV/Visible spectroscopy, would tend to move the two copper ions closer and then to favour exchange interaction between them.

Conclusions

The dinuclear Cu^{II} and Ni^{II} complexes based on biscyclen $\mathbf{L^{1,2}}$ or biscyclam $\mathbf{L^{3,4}}$ ligands have been studied. X-ray analysis of copper biscyclen complexes have shown that the pyridyl nitrogen atom [N(*py*)] coordinates one of the two copper ions. In solution, the comparison of the UV/Visible spectra of these two complexes indicates that the coordination of the N(*py*) atom is maintained, even upon acidification. The coordination of the N(*py*) atom leads to the shortening of the intermetallic copper–copper distance: as a result, the dipolar intermetallic interaction is promoted. This is underlined by the EPR spectrum of $[Cu_2\mathbf{L^2}]^{4+}$ complex, which exhibits in the parallel region nine equidistant lines (against seven for $[Cu_2\mathbf{L^1}]^{4+}$).

For the cyclam complexes, no evidence of the N(*py*) atom coordination to one of the two metal centres was found. However, EPR spectra of these dinuclear copper complexes show that a weak intermetallic interaction is still present since the parallel region of the spectra present seven equidistant lines. Nevertheless, for the corresponding nickel biscyclam complexes, electrochemical oxidation–reduction cycles, which promote a configurational rearrangement between type III and type I configurations of Ni biscyclam, can induce a coordination of the N(*py*) atom in the type I geometry. In this case, the strengthening of the metal–metal interaction is suggested by the splitting of the corresponding CV traces.

From this study, one can conclude that the existence of a potentially coordinating atom on the intercycle spacer can improve the metal–metal interaction. Consequently, bismacrocycles possessing more than one potentially coordinating atom on the spacer are currently under study.

Experimental Section

Syntheses: The metals salts were purchased from Aldrich. The other reagents were used as highest grade commercially available without further purification.

Ligand Synthesis: The synthesis and the characterisation of ligands $\mathbf{L^1}$ and $\mathbf{L^3}$ have been described previously elsewhere.[7] Ligands $\mathbf{L^2}$ and $\mathbf{L^4}$ have been synthesised according to the same procedure from cyclen or cyclam glyoxal ligands and 2,6-bis(bromomethyl)-pyridine.[26]

Ligand $\mathbf{L^2}$: Yield 69%. ^{13}C NMR ($CDCl_3$): δ = 44.4, 45.6, 46.3, 51.2, 60.5 (CH_2N), 121.1, 136.6, 158.4 (C_{ar}). Elemental analysis calcd. (%) for the hydrochloride salt of L^2: $C_{23}H_{45}N_9 \cdot 6HCl \cdot H_2O$: C 40.36, H 7.81, N 18.42; found: C 40.23, H 7.76, N 18.17.

Ligand $\mathbf{L^4}$: Yield 71%. ^{13}C NMR ($CDCl_3$): δ = 26.2–28.7 (CH_2CH_2N), 47.3, 47.9, 48.8, 49.1, 50.6, 53.2, 55.3, 59.5 (CH_2N), 120.9, 136.3, 158.6 (C_{ar}). Elemental analysis calcd. (%) for the hydrochloride salt of L^4: $C_{27}H_{53}N_9 \cdot HCl \cdot 2H_2O$: C 42.75, H 8.37, N 16.62; found: C 42.99, H 8.11, N 16.45.

Synthesis of $Cu_2L^1(ClO_4)_4{\cdot}4H_2O$: The neutral ligand ($5.2{\cdot}10^{-5}$ mol) was dissolved in distilled water (10 mL) followed by the addition of an ethanolic solution of the copper(II) perchlorate salt ($1.17{\cdot}10^{-4}$ mol). The blue solution was refluxed for 2 h and the solvents were evaporated under vacuum. The solid was washed twice with absolute ethanol. Elemental analysis calcd. (%) for $C_{24}H_{54}Cl_4Cu_2N_8O_{20}$: C 27.62, H 5.21, N 10.74; found: C 27.99, H 5.14, N 10.45.

This solid was further dissolved in water and the diffusion of an aqueous saturated sodium perchlorate solution produced monocrystals of $[Cu_2L^1(H_2O)_2](ClO_4)_4{\cdot}H_2O$, suitable for X-ray analysis.

Synthesis of $Cu_2L^{1-4}(BF_4)_4$ and $Ni_2L^{1-4}(BF_4)_4$: The neutral ligands ($5.2\ 10^{-5}$ mol) were dissolved in distilled water (10 mL) and aqueous solutions of copper(II) or nickel (II) salts ($1.17\ 10^{-4}$ mol in 5 mL) were added dropwise. The resulting solutions were heated at reflux for 2 h, the solvents were evaporated under vacuum afterwards. The solids were washed twice with absolute ethanol.

Elemental analysis for $Cu_2L^1(BF_4)_4{\cdot}2H_2O$: $C_{24}H_{50}B_4Cu_2N_8F_{16}O_2$ calcd. (%): C 30.12, H 5.27, N 11.71; found: C 29.99, H 5.02, N 12.39. $Cu_2\mathbf{L^2}(BF_4)_4$, $3H_2O$ $C_{23}H_{51}B_4Cu_2N_9F_{16}O_3$ calcd. (%): C 28.30, H 5.27, N 12.92; found: C 28.22, H 4.83, N 12.67. $Cu_2\mathbf{L^3}(BF_4)_4$ $C_{28}H_{54}B_4Cu_2N_8F_{16}$ calcd. (%): C 34.42, H 5.57, N 11.47; found: C 34.78, H 5.60, N 11.53. $Cu_2\mathbf{L^4}(BF_4)_4$, $2H_2O$ $C_{27}H_{57}B_4Cu_2N_9F_{16}O_2$ calcd. (%): C 31.98, H 5.67, N 12.43; found: C 32.17, H 5.32, N 11.90.

$Ni_2\mathbf{L^1}(BF_4)_4{\cdot}1H_2O$: $C_{24}H_{48}B_4Ni_2N_8F_{16}O$ calcd. (%): C 31.02, H 5.21, N 12.06; found: C 30.73, H 5.61, N 12.36. $Ni_2\mathbf{L^2}(BF_4)_4$, $C_{23}H_{45}B_4Ni_2N_9F_{16}$ calcd. (%): C 30.28, H 4.97, N 13.82, found: C 30.61, H 5.34, N 13.69. $Ni_2\mathbf{L^3}(BF_4)_4$, $3H_2O$ $C_{28}H_{60}B_4Ni_2N_8F_{16}O_3$ calcd. (%): C 32.94, H 5.92, N 10.97; found: C 32.85, H 5.58, N 10.34. $Ni_2\mathbf{L^4}(BF_4)_4$, $2H_2O$ $C_{27}H_{57}B_4Ni_2N_9F_{16}O_2$ calcd. (%): C 32.29, H 5.72, N 12.55; found: C 32.34, H 5.08, N 11.99.

Crystals of $Cu_2\mathbf{L^2}(BF_4)_4$ suitable for X-ray crystallography were obtained by slow diffusion of diethyl ether into an acetonitrile solution of the complex.

Spectroscopic Measurements: Electronic spectra in aqueous or acetonitrile solutions (10^{-3} mol L^{-1}) were all measured in the 300–900 nm range with a Lambda 6 Perkin–Elmer spectrophotometer. The acetonitrile solution of trifluoroacetic acid (0.1 mol L^{-1}) was prepared by dilution of trifluoroacetic acid Aldrich product at 99%. The acidification of acetonitrile copper complex solutions was obtained by successive additions of trifluoroacetic acid solution (100 μL).

The X-band EPR spectra (9.40 GHz) were recorded in DMF solutions at 100 K, with a Bruker spectrophotometer ELEXSYS 500. Simulations were carried out using the software Simfonia.[25]

Electrochemical Measurements: Voltammetric data were recorded with an Autolab with a PGSTAT12 potentiostat (ECO Chemie) associated to a conventional three electrodes electrochemical cell, the working electrode being a glassy carbon or platinum disk, a platinum plate being used as a counter electrode and in aqueous medium a saturated calomel electrode was used as the reference while in acetonitrile a silver electrode separated from the complex solution was used as a pseudo reference. In acetonitrile, the potential of the pseudo reference was measured vs. the ferricinium/ferrocene couple. Complexes concentrations were always close to 10^{-3} mol L^{-1} and in acetonitrile tetrabutylammonium hexafluorophosphate 10^{-1} mol L^{-1} was used as the supporting electrolyte. In concentrated perchloric acid solutions no additional electrolyte was employed.

Computational Details: The calculations have been performed using the Gaussian 98[27] program package. Both geometry and energy calculations were performed at the UHF/LANL2 MB level. Each molecular structure has been fully optimised and characterised as minimum by frequency analysis. Single point energy have further been calculated at the UB3LYP/LANL2DZ level [the LANL2DZ basis set as parameterised in Gaussian has been supplemented with polarisation function on nitrogen atoms (d_N = 0.80)].

Crystal Structure Determination: The crystal data were collected at 173 K with a Kappa CCD diffractometer using monochromated Mo-K_α radiation (λ = 0.71073 Å).

Table 5. Crystal data and details of the structure determination for $[Cu_2\mathbf{L^1}](ClO_4)_4$ and $[Cu_2\mathbf{L^2}\ BF_4]\ (BF_4)_3$.

	$[Cu_2\mathbf{L^1}](ClO_4)_4(H_2O)_3$	$[Cu_2\mathbf{L^2}\ BF_4](BF_4)_3$
Empirical formula	$C_{24}\ H_{52}\ N_8\ O_{19}\ Cl_4\ Cu_2$	$C_{23}\ H_{45}\ N_9\ B_4\ F_{16}\ Cu_2$
Formula mass	1025.62	921.97
Temperature [K]	173	173
Crystal system	monoclinic	orthorhombic
Space group	$P12_{1/n}1$	*Pbca*
Color	blue	blue
a [Å]	14.9096(3)	20.1554(2)
b [Å]	8.8632(2)	20.2243(3)
c [Å]	30.7758(6)	17.7403(2)
α [°]	90	90
β [°]	96.913(5)	90
γ [°]	90	90
Volume [Å^3]	4037(1)	7231.5(2)
Z	4	8
$D_{calcd.}$ [g cm^{-3}]	1.69	1.69
Absorption coefficient [mm^{-1}]	1.402	1.292
F(000)	2120	3744
λ (Mo-K_α) [Å]	0.71073	0.71073
No independent reflections	9584	11472
No reflcns. [$I > 3.0\ \sigma(I)$]	4599	4506
*R*1	0.056	0.072
wR_2	0.080	0.085
Goodness-of-fit on F^2	1.442	1.200

The structures were solved by direct methods. After refinement of the non-hydrogen atoms, difference-Fourier maps revealed maxima of residual electron density close to positions expected for hydrogen atoms. Hydrogen atoms were introduced as fixed contributors at calculated positions [C–H = 0.95 Å, B(H) = 1.3 B_{eqv}]. Final difference maps revealed no significant maxima. All calculations were using the Nonius OpenMoleN package.[28] Neutral atom scattering factor coefficients and anomalous dispersion coefficients were taken from a standard source.

CCDC-261457 (for $[Cu_2\mathbf{L^1}(H_2O)_2]\cdot 4ClO_4\cdot 3H_2O$) and CCDC-261458 (for $[Cu_2\mathbf{L^2}BF_4]\cdot 3BF_4$) contains the supplementary crystallographic data for this paper. These data can be obtained free of charge from The Cambridge Crystallographic Data Centre via www.ccdc.cam.ac.uk/data_request/cif.

Crystal data and details of the structure determination for $[Cu_2\mathbf{L^1}]\cdot(ClO_4)_4$ and $[Cu_2\mathbf{L^2}BF_4]\cdot(BF_4)_3$ are given in the following Table 5.

Acknowledgments

We thank Dr. A. de Cian (Université Louis Pasteur, Strasbourg, France) for the single-crystal X-ray analyses, Dr. Y. Frappart (Université René Descartes, Paris, France) for the EPR spectra. Dr. E. Derat (Université de Reims Champagne Ardenne, France) is gratefully acknowledged for helpful discussions in molecular modelling as well as the computational centre of "Université de Reims Champagne Ardenne" for computational facilities.

[1] A. Bianchi, M. Micheloni, P. Paoletti, *Coord. Chem. Rev.* **1991**, *110*, 17.
[2] a) J. R. Morphy, D. Parker, R. Alexander, A. Bains, M. A. W. Eaton, A. T. Millican, K. Titmas, D. J. Weatherby, *J. Chem. Soc. Chem. Commun.* **1988**, 156; b) J. R. Morphy, D. Parker, R. Kataky, M. A. W. Eaton, A. T. Millican, A. Phipps, C. J. Walker, *J. Chem. Soc. Chem. Commun.* **1989**, 792.
[3] A. E. Merbach, E. Tóth (Eds.), *The Chemistry of Contrast Agents in Medical Magnetic Resonance Imaging*, Wiley, Chichester, **2001**.
[4] a) A. Mc.Auley, S. Subramanian, *Inorg. Chem.* **1997**, *36*, 5376; b) A. McAuley, S. Subramanian, M. J. Zawarotko, K. Biradha, *Inorg. Chem.* **1999**, *38*, 5078; c) M. Lachkar, R. Guilard, A. Atmani, A. De Cian, J. Fischer, R. Weiss, *Inorg. Chem.* **1998**, *37*, 1575; d) P. Comba, Y. D. Lampeka, L. Lötzbeyer, A. I. Prikhod'ko, *Eur. J. Inorg. Chem.* **2003**, 34; e) A. Bencini, E. Berni, A. Bianchi, C. Giorgi, B. Valtancoli, D. K. Chand, H. J. Schneider, *Dalton Trans.* **2003**, 793; f) Y. Dong, L. F. Lindoy, P. Turner, G. Wei, *Dalton Trans.* **2004**, 1264.
[5] a) L. Fabbrizzi, F. Forlini, A. Perotti, B. Seghi, *Inorg. Chem.* **1984**, *23*, 807; b) R. Schneider, A. Riesen, T. A. Kaden, *Helv. Chim. Acta* **1986**, *69*, 53; c) L. Fabbrizzi, L. Montagna, A. Poggi, T. A. Kaden, Siegfried, *Inorg. Chem.* **1986**, *25*, 2672; d) M. Ciampolini, L. Fabbrizzi, A. Perotti, A. Poggi, B. Seghi, F. Zanobini, *Inorg. Chem.* **1987**, *26*, 3527; e) L. Fabbrizzi, L. Montagna, A. Poggi, T. A. Kaden, Siegfried, *J. Chem. Soc., Dalton Trans.* **1987**, 2631; f) T. A. Kaden, *Coord. Chem. Rev.* **1999**, *190–192*, 371.
[6] a) D. T. Pierce, T. L. Hatfield, E. J. Billo, Y. Ping, *Inorg. Chem.* **1997**, *36*, 2950; b) C. Amatore, J. M. Barbe, C. Bucher, E. Duval, R. Guilard, J. N. Verpeaux, *Inorg. Chim. Acta* **2003**, *356*, 267; c) C. Bucher, J. C. Moutet, J. Pécaut, G. Royal, E. Saint-Aman, F. Thomas, *Inorg. Chem.* **2004**, *43*, 3777.
[7] M. Le Baccon, F. Chuburu, L. Toupet, H. Handel, M. Soibinet, I. Déchamps-Olivier, J. P. Barbier, M. Aplincourt, *New J. Chem.* **2001**, *25*, 1168.
[8] M. Soibinet, I. Déchamps-Olivier, E. Guillon, J. P. Barbier, M. Aplincourt, F. Chuburu, M. Le Baccon, H. Handel, *Eur. J. Inorg. Chem.* **2003**, 1984.
[9] A. E. Goeta, J. A. K. Howard, D. Maffeo, H. Puschmann, J. A. Gareth Williams, D. S. Yufit, *J. Chem. Soc., Dalton Trans.* **2000**, 1873.
[10] Y. Dong, G. A. Lawrence, L. F. Lindoy, P. Turner, *Dalton Trans.* **2003**, 1567.
[11] B. J. Hathaway, A. A. G. Tomlinson, *Coord. Chem. Rev.* **1970**, *5*, 1.
[12] K. Miyoshi, T. Tanaka, E. Kimura, S. Tsuboyama, S. Murata, H. Shimizu, K. Ishizu, *Inorg. Chim. Acta* **1983**, *78*, 23.
[13] H. Kurosaki, C. Bucher, E. Espinosa, J. M. Barbe, R. Guilard, *Inorg. Chim. Acta* **2001**, *322*, 145.
[14] T. Yokoyama, H. Kitagawa, H. A. Iwasawa, M. Zenki, *Inorg. Chim. Acta* **1996**, *253*, 1.
[15] L. Sabatini, L. Fabbrizzi, *Inorg. Chem.* **1979**, *18*, 438.
[16] a) A. Bencini, L. Fabbrizzi, A. Poggi, *Inorg. Chem.* **1981**, *20*, 2544; b) A. Buttafava, L. Fabbrizzi, A. Perotti, A. Poggi, G. Poli, B. Seghi, *Inorg. Chem.* **1986**, *25*, 1456.
[17] a) L. Fabbrizzi, *Comments Inorg. Chem.* **1986**, *25*, 4197; b) C. Bisi Castellani, M. Licchelli, A. Perotti, A. Poggi, *J. Chem. Soc., Chem. Commun.* **1984**, 806; c) F. V. Lovecchio, E. S. Gore, D. H. Busch, *J. Am. Chem. Soc.* **1974**, *96*, 3109.
[18] E. Kimura, T. Koike, R. Machida, R. Nagai, M. Kodama, *Inorg. Chem.* **1984**, *23*, 4181.
[19] B. Bonisch, C. K. Poon, M. L. Tobe, *Inorg. Chem.* **1965**, *4*, 1102.
[20] M. A. Donnelly, M. Zimmer, *Inorg. Chem.* **1999**, *38*, 1650.
[21] X. Liang, J. A. Parkinson, M. Weishäupl, R. O. Gould, S. J. Paisey, H. Park, T. M. Hunter, C. A. Blindauer, S. Parsons, P. J. Sadler, *J. Am. Chem. Soc.* **2002**, *124*, 9105.
[22] S. Brandès, C. Gros, F. Denat, P. Pullumbi, R. Guilard, *Bull. Soc. Chim. Fr.* **1996**, *133*, 65.
[23] B. J. Hatthaway, D. E. Billing, *Coord. Chem. Rev.* **1970**, *5*, 143.
[24] E. F. Hasty, L. J. Wilson, D. N. Henrickson, *Inorg. Chem.* **1978**, *17*, 1834.
[25] Simfonia, EPR Data Analysis and Simulation, **1994–96**, Bruker.
[26] M. A. Reppy, M. E. Cooper, J. L. Smithers, D. L. Gin, *J. Org. Chem.* **1999**, *64*, 4191.
[27] M. J. Frisch, G. W. Trucks, H. B. Schlegel, G. E. Scuseria, M. A. Robb, J. R. Cheesemen, V. G. Zakrzewski, J. A. Montgomery, R. E. Stratmann, J. C. Burant, S. Dapprich, J. M. Millam, A. D. Daniels, K. N. Kudin, M. C. Strain, O. Farkas, J. Tomasi, V. Barone, M. Cossi, R. Cammi, M. Mennucci, C. Pomelli, C. Adamo, S. Clifford, J. Ochterski, G. A. Petersson, P. Y. Ayala, Q. Cui, K. Morokuma, D. K. Malik, A. D. Rabuk, K. Raghavachari, J. B. Foresman, J. Cioslowski, J. V. Ortiz, B. B. Stefanov, G. Liu, A. Liashenko, P. Piskorz, I. Komaromi, R. Gomperts, R. L. Martin, D. J. Fox, T. Keith, M. A. Al-Laham, C. Y. Peng, A. Nanayakkara, G. Gonzalez, M. Challacombe, P. M. W. Gill, B. G. Johnson, W. Chen, M. W. Wong, J. L. Andres, M. Head-Gordon, E. S. Replogle, J. A. Pople, *Gaussian 98* (Revision A.1), Gaussian, Inc. Pittsburg PA, **1998**.
[28] *OpenMoleN*, Interactive Structure Solutions, B. V., Nonius Delft, The Netherlands, **1997**.

Received: February 8, 2005

